



Graphitic-N highly doped graphene-like carbon: A superior metal-free catalyst for efficient reduction of CO₂

Jingjing Li^a, Wen-Yan Zan^a, Hongxing Kang^b, Zhengping Dong^{c,*}, Xiaoming Zhang^a, Yixiong Lin^b, Yue-Wen Mu^a, Fengwei Zhang^{a,b,**}, Xian-Ming Zhang^{a,*}, Jing Gu^{b,*}

^a Institute of Crystalline Materials, Institute of Molecular Science, Shanxi University, Taiyuan, 030006, PR China

^b Department of Chemistry and Biochemistry, San Diego State University, 5500 Campanile Drive, San Diego, CA, 92182-1030, USA

^c College of Chemistry and Chemical Engineering, Lanzhou University, Lanzhou, 730000, PR China

ARTICLE INFO

Keywords:

Phthalocyanine
Soft template
N-doped graphene-like carbon
CO₂ electroreduction
Active site

ABSTRACT

For metal-free nitrogen(N)-doped carbon catalysts, diverse N-bearing species embedded in the carbon framework are generally regarded as chemical promoters that can upgrade their catalytic performance for CO₂ electroreduction reaction (CO₂RR). However, it is still a controversy as to which N species plays a dominant role. Herein, a type of large surface area (371 m²/g), N-rich (11.0 wt%) graphene-like carbon electrocatalyst (NG-1000) is fabricated via facile pyrolysis from a precursor composite of dicyandiamide and phthalocyanine. The N-species in the NG-T (T = 700–1000 °C) can be fine-tuned, thus facilitating differentiating functions of the various N-species. Based on the comprehensive analysis of original Pc/CNTs and NG-T catalysts, we identified that the C atoms next to the graphitic-N species in NG-1000 serves as the main active species for CO₂RR. In addition, such a non-metal based electrocatalyst is capable of achieving an excellent selectivity of 95.0 % at –0.72 V versus RHE to convert CO₂ into CO, with a CO current density of 9.07 mA cm⁻², comparable to the state-of-the-art metal-based electrocatalysts.

1. Introduction

The electrochemical CO₂ reduction reaction (CO₂RR) is a promising avenue to convert CO₂ into high value-added fuels and commodity chemicals [1,2]. Hitherto, not only C₁ products (CO, CH₄, HCOOH and CH₃OH) but also multi-carbon products (C₂H₄, C₂H₅OH and CH₃COCH₃, etc.) have been produced by various noble/non-noble metal-based CO₂RR catalysts [3–6]. Among these products, CO molecule is considered to be an attractive and competitive feedstock for downstream chemical transformation, such as carbonylation, hydroformylation and Fischer-Tropsch synthesis [7–9]. It has been demonstrated that the selective preparation of CO by CO₂RR can be effectively promoted by metallic porphyrin/phthalocyanine-based MOFs, COFs materials as well as single-atom catalysts supported on N-doped carbon [10–16]. Given that the limited reserves of metal resources, together with the uncertainties of whether other non-metal atoms have also participated in the catalytic conversion process, it is necessary to develop heteroatom-doped non-metal catalysts, explore their chemical nature,

and unravel their catalytic mechanisms.

The heteroatom (N, F, P, S etc.) doped carbon has recently proved to be a powerful heterogeneous catalyst. The activity of these carbon-based materials may be inferior to metal-based catalysts, but their abundance, accessibility, and low cost have attracted tremendous attention [17–20]. In particular, N-doped carbon nanomaterials have demonstrated superior catalytic activities towards various ORR, OER, hydrogenation of nitroarenes, Knoevenagel reaction and oxidative cleavage of benzylic C–H bond [21–24]. Since Salehi-Khojin's group firstly reported metal-free carbon nanofibres as an effective catalyst for CO₂RR in ionic liquid, several other references on N-doped carbon catalysts fabricated via different C, N-containing precursors were disclosed and investigated [25]. For instance, Zhou et al. synthesized a series of N-doped carbon nanotubes using CH₃CN, DMF and TEA as precursors to adjust the configuration and contents of the N containing species. In this work, the authors proposed that both pyridinic and graphitic-N are active sites for CO₂RR because those two N species are indistinguishable [26]. Liu et al. elaborately designed a set of 3D N-doped graphene nanoribbon

* Corresponding authors.

** Corresponding author at: Institute of Crystalline Materials, Institute of Molecular Science, Shanxi University, Taiyuan, 030006, PR China.

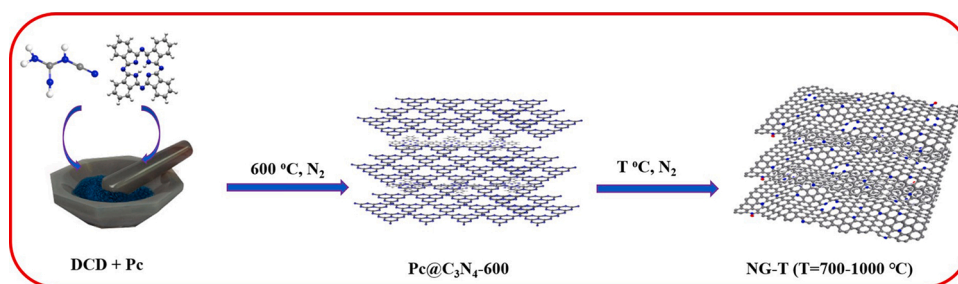
E-mail addresses: dongzhp@lzu.edu.cn (Z. Dong), fwzhang@sxu.edu.cn (F. Zhang), xmzhang@sxu.edu.cn (X.-M. Zhang), jgu@sdsu.edu (J. Gu).

<https://doi.org/10.1016/j.apcatb.2021.120510>

Received 25 March 2021; Received in revised form 22 June 2021; Accepted 5 July 2021

Available online 6 July 2021

0926-3373/© 2021 The Authors. Published by Elsevier B.V. This is an open access article under the CC BY license (<http://creativecommons.org/licenses/by/4.0/>).



Scheme 1. The synthetic procedure for metal-free N-doped graphene-like carbon catalyst (NG-T).

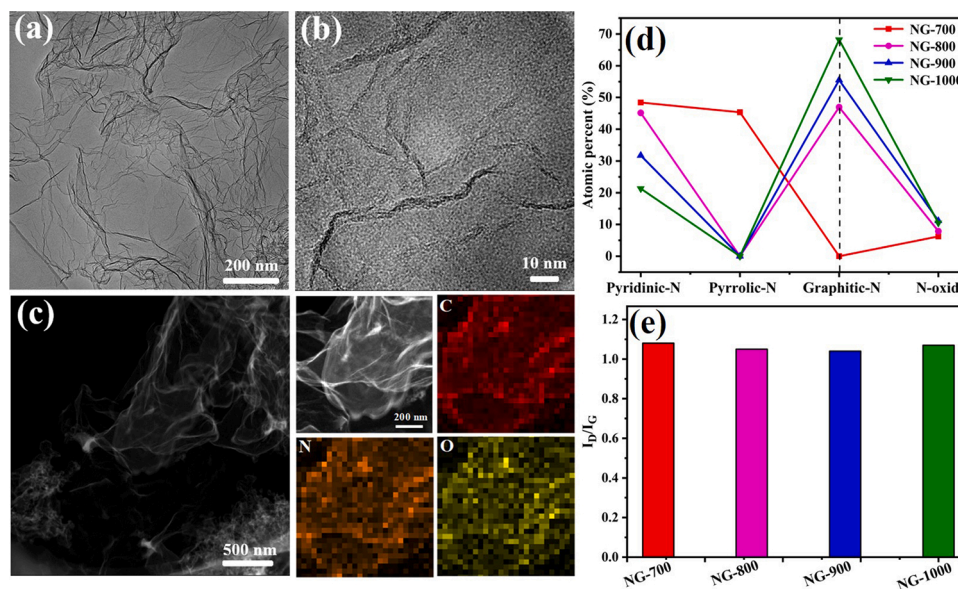


Fig. 1. (a) TEM, (b) HRTEM, (c) HAADF-STEM and elemental mapping images of NG-1000, (d) the, respectively, N species content under various pyrolysis temperatures. (e) I_p/I_g ratio of NG-T under various pyrolysis temperatures.

(N-GRW) with tunable N dopants to reveal the site-dependent CO₂RR activity and selectivity, where they hold the view that the pyridinic N site in N-GRW should be the active site [27]. Although N-doped carbon has been reported to possess excellent CO selectivity in CO₂RR, their current density is generally low and the selectivity needs to be further improved [28–30]. Besides, the active sites for CO₂RR are somewhat controversial because different types of N species are simultaneously embedded in the skeleton of the carbon frameworks in the aforementioned catalytic materials. Therefore, it is crucial to fabricate a 2D N-doped carbon with highly exposed active sites and distinguishable N species to address the above challenges.

Metal phthalocyanine (MPc) and its derived conjugated microporous polymer are identified as the ideal precursors for fabricating carbon-based catalysts due to their exceptional properties, such as the high N content, conjugated planar structure for efficient charge transfer, and well-isolated metal sites [31–35]. However, the direct pyrolysis of MPc itself only yields N-doped carbon materials with poor porosity and low surface area, limiting their catalytic performance. Recently, multiple hard and soft templates, such as silica, zeolites, cellulose, organic polymers and surfactants were mixed with MPc and its derivatives in the pyrolysis process to improve the porosity and surface area of N-doped carbon materials [36]. But the toxicity of etching agents and complicated mixing procedures restrain their production at a large scale. Interestingly, dicyandiamide (DCD) is a widely used precursor for the preparation of graphite carbon nitride (g-C₃N₄), which can be completely decomposed at higher temperatures (> 700 °C), thus effectively avoiding the tedious template removal process [37]. Based on the

above considerations, herein a series of N-doped graphene-like carbon deriving from one-step pyrolysis of Pc and dicyandiamide (DCD) is reported. The resulting NG-T (T = 700–1000 °C) catalysts not only display thin graphene-like carbon structures decorated with identifiable N species, but also have high surface areas (246–371 m²/g) and rich N content (11.0–33.7 %), which eventually result in excellent catalytic performance for CO₂RR.

2. Experimental

2.1. Materials

Phthalocyanine was purchased from Tokyo Chemical Industry Co., Ltd. Dicyandiamide was obtained from Aladdin Biochemical Technology Co., Ltd. Potassium bicarbonate (KHCO₃, 99.7 %) was purchased from Sigma-Aldrich. All reagents were used directly, without further purification. Deionized water was used as the solvent throughout the catalytic experiments.

2.2. Synthesis of NG-T catalyst

50 mg of phthalocyanine and 1.0 g of dicyandiamide (mass ratio = 20:1) were mixed and repeatedly ground to form a homogeneous light blue powder. The composites were transferred into a tubular furnace reactor and were pyrolyzed for 2 h (heating rate: 3 °C/min) under the flowing N₂ at the set temperature. After naturally cooling down to room temperature, the resultant black powder denoted as NG-T (T is the

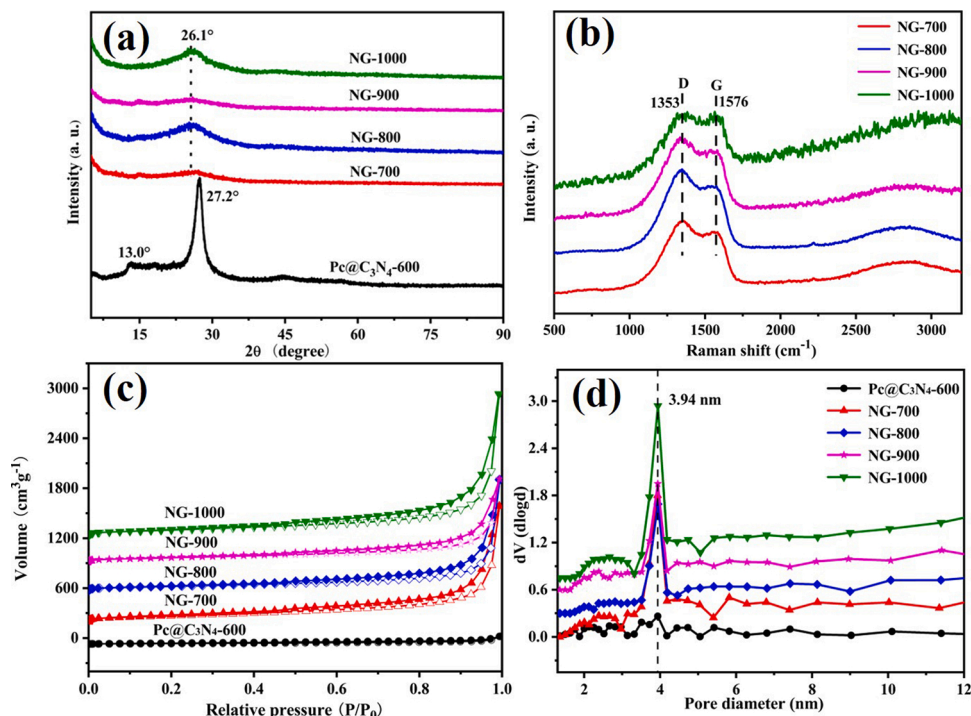


Fig. 2. (a) XRD patterns, (b) Raman spectra, (c) N_2 adsorption-desorption isotherms and (d) the corresponding pore size distribution curves of NG-T catalyst (T = 700–1000 °C).

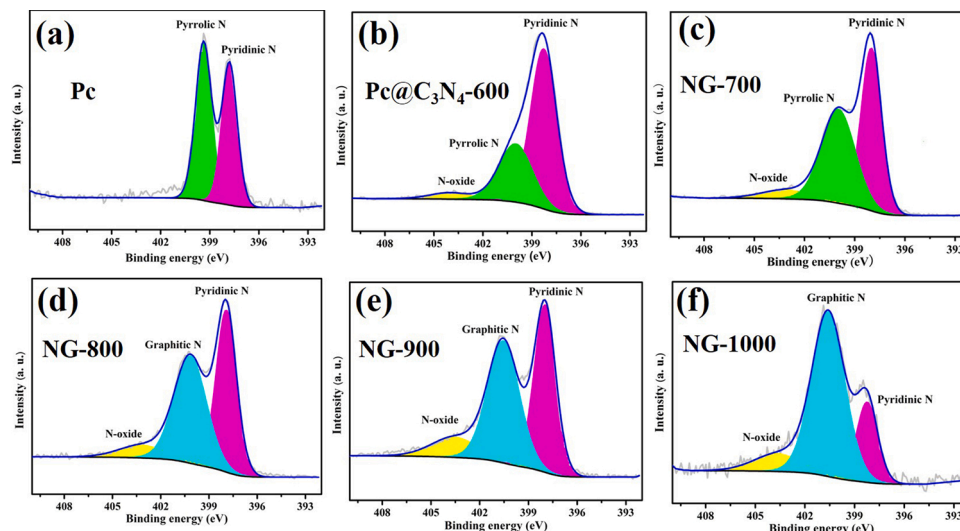


Fig. 3. High-resolution XPS analysis in $N1s$ region of (a) Pc parent, (b) $Pc@C_3N_4-600$, (c) NG-700, (d) NG-800, (e) NG-900 and (f) NG-1000 catalysts.

pyrolysis temperature, NG refers to the N-doped graphene-like carbon) was obtained without further treatment.

2.3. Synthesis of Pc/CNTs catalyst

The as-received 0.5 g of CNTs were dispersed in 80 mL of concentrated HNO_3 solution and sonicated for 30 min, and then it was refluxed at 110 °C for 2 h. After cooling to room temperature, the purified CNTs were collected by filtration and washed extensively with the deionized water. Subsequently, 30 mg of the purified CNTs were dispersed in 30 mL of DMF using sonication. Further, 3.0 mg of Pc dissolved in DMF was added to the CNTs suspension. The mixture was stirred at room temperature for 24 h after sonication for 30 min. Subsequently, the mixture was centrifuged, and the precipitate was washed with DMF and ethanol.

Finally, the precipitate was lyophilized to yield the Pc/CNTs control sample.

2.4. Electrochemical CO_2RR measurement

Electrochemical CO_2RR was conducted using a three-electrode configuration in a 0.5 M $KHCO_3$ solution saturated with high-purity CO_2 gas at room temperature. Platinum wire and Ag/AgCl (0.21 V vs. normal hydrogen electrode (NHE), Model RE-5B, BASI, USA) was used as the counter electrode and reference electrode, respectively. The potentials were controlled by an electrochemical workstation (CHI 630) and then converted to reversible hydrogen electrode (RHE) according to the equation: $E_{RHE} = E_{Ag/AgCl}^0(0.21) + E_{Ag/AgCl} + 0.059 \cdot pH$. Before the electrochemical test, CO_2 gas was purged into the $KHCO_3$ solution for 30

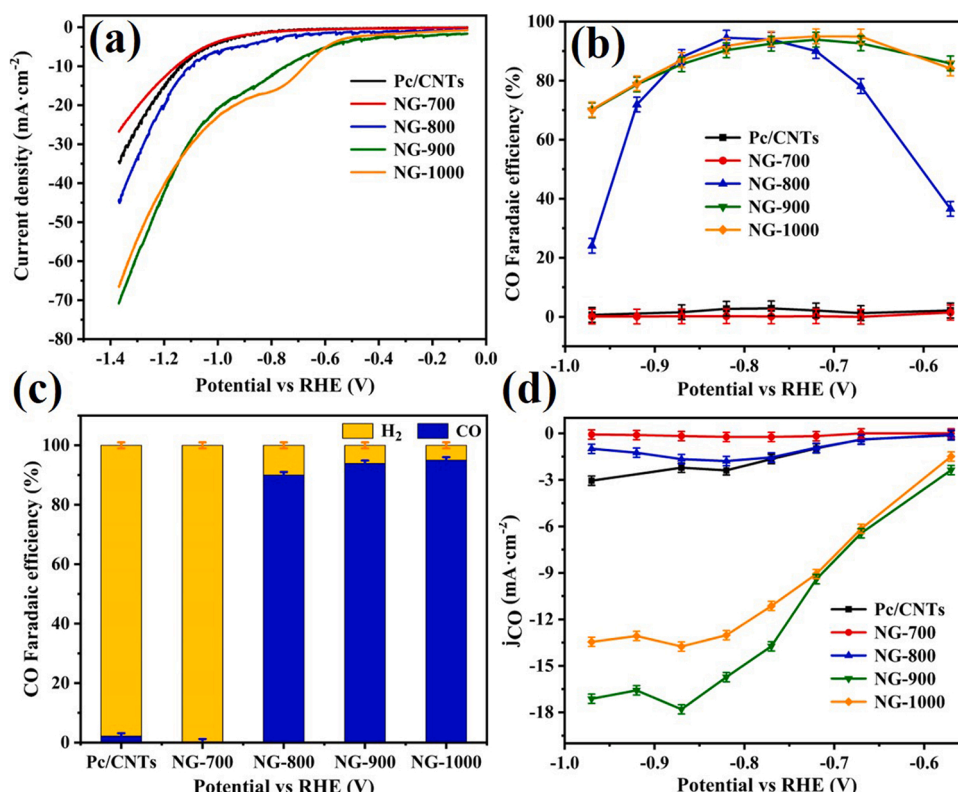


Fig. 4. (a) Linear sweep voltammetry curves of Pc/CNTs and NG-T catalysts, (b) Faradaic efficiency for CO₂RR with Pc/CNTs and NG-T catalysts at different potentials, (c) Comparison of the product selectivity for different catalysts at -0.72 V versus RHE, (d) Partial current density for CO formation at different potentials.

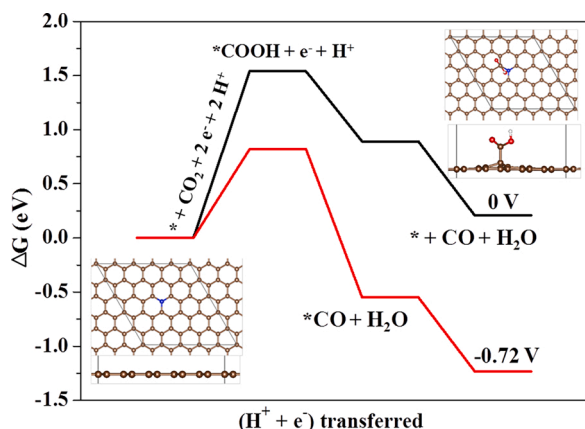


Fig. 5. The calculated free energy diagram for CO₂RR to CO on NG-1000 catalyst (black: the lowest energy pathway at 0 V vs. RHE, Red: at an applied potential of -0.72 V vs. RHE).

min with a flow rate of 20 sccm to remove the residual air in the electrolyzer. Controlled potentiostatic electrolysis was carried out at each potential for 30 min, the composition and distribution of gas products were analyzed by gas chromatography (SHIMADZU, GC-2010) equipped with a BID detector at 10 min intervals. In this work, the average result from three trials was reported. The stability of NG-1000 catalyst was investigated by continuous 10 h electrolysis and the gaseous products were analyzed by GC at 1 h intervals. The CO/H₂ Faradaic efficiency and partial current density were calculated by using the following equations: $FE_{CO} = C_{CO} * S * (2 F P / RT) / I_{total}$, $FE_{H_2} = C_{H_2} * S * (2 F P / RT) / I_{total}$;

$$j_{CO} = C_{CO} * S * (2 F P / RT) / A, j_{H_2} = C_{H_2} * S * (2 F P / RT) / A$$

C_{CO} , and C_{H_2} are the concentration of CO and H₂ measured with GC, S is

the flow rate of CO₂ (10 sccm), F is the Faradaic constant, P is the atmospheric pressure, T is the thermodynamic temperature (298.15 K), R is the gas constant (8.314 J mol⁻¹ K⁻¹), I_{total} is the measured current, A is the volumetric area of the electrode.

2.5. Characterization

Transmission electron microscope (TEM) was carried out on a FEI Tecnai G2 F20S-Twin using an accelerating voltage of 200 kV. For sample preparation, the powders were dispersed in ethanol via ultrasonication, and one drop of the solution was dropped onto a micro grid. Atomic Force Microscopy (AFM) was carried out on a Multimode 8. The AFM sample was prepared by dropping cast catalysts dispersed in ethanol onto a clean surface of mica and dried at room temperature. XRD measurements were performed on a Rigaku Ultima IV diffractometer using Cu-K α radiation in the 2θ range of 5–90°. The N₂ adsorption-desorption isotherms were obtained on an ASAP2020 analyzer. Before measurement, samples were degassed under vacuum at 393 K for 6 h. The surface area of the samples was calculated by the Brunauer-Emmet-Teller (BET) method, and pore volume and size distribution were calculated using the Barrett-Joyner-Halenda (BJH) model. Fourier transform infrared (FTIR) spectra were obtained using a Nicolet iS5 spectrophotometer (frequency range from 4000 to 400 cm⁻¹) with KBr pellet. The X-ray photoelectron spectra (XPS) were analyzed by the PHI-5702 instrument and the C1s line at 284.5 eV was used as the binding energy reference.

3. Results and discussion

3.1. Microstructure characterization of NG-T catalyst

The general procedure for fabricating NG-T catalyst (T is the pyrolysis temperature) is shown in Scheme 1. Briefly, Pc and DCD with different mass ratios are mechanically ground followed by pyrolysis

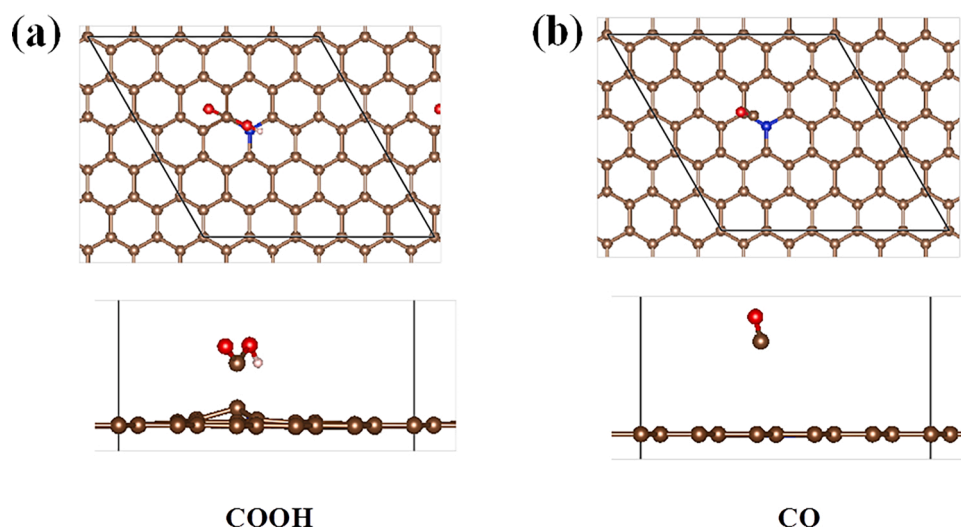


Fig. 6. The most stable structures of (a) *COOH and (b) *CO intermediates adsorbed on NG-1000 catalyst.

under the N_2 protection. During this process, the DCD monomer will transform to g- C_3N_4 hard template which in-situ surrounds the Pc and its prepolymer, generating a sandwich-like stacking structure below 600 °C as shown in Scheme 1. When the pyrolysis temperature further elevated to above 700 °C, the graphitization of Pc-based polymer and decomposition of g- C_3N_4 template will take place simultaneously. Notably, the volatile N-containing species released by the decomposition of g- C_3N_4 can be incorporated into the graphene-like carbon skeleton, increasing the N contents and defects amount in the resultant catalysts [38]. Considering that this process can obviously reduce the layers of graphitic carbon and the generation of more exposed active sites, such DCD soft-template assisted strategy is ideal for the preparation of efficient N-doped graphene-like carbon catalysts.

TEM images of representative NG-1000 catalyst are shown in Fig. 1a–b. As predicted, it presents a typical wrinkled lamellar architecture with an extremely thin thickness under DCD soft template-assisted pyrolysis conditions. HAADF-STEM and EDS mapping images demonstrate that the C, N and O elements are homogeneously distributed in the graphene-like carbon skeleton (Fig. 1c). AFM characterization further corroborates the average thickness of the graphene-like carbon to be 2.51 nm, approximated to 7–8 layers of graphene, confirming the feasibility of such soft template-assisted strategy to create ultra-thin carbon skeletons (Fig. S1). Fig. 1d–e reveals the content of graphitic-N is significantly increased from 0 to 68.2 wt% under increased pyrolysis temperatures, while the I_D/I_G ratio is initially decreased and then increased with the increasing temperature from 700 °C to 1000 °C. The results prove that the amounts of N species, specially the graphitic-N and degrees of defect in NG-T catalyst can be fine-tuned by the pyrolysis temperature. The content of graphitic-N will be further used to correlate with the catalytic properties of N-doped carbon catalysts.

XRD patterns of NG-T samples illustrate the phase transformation during the pyrolysis process of Pc and DCD (Fig. 2a). Once the pyrolysis temperatures are above 700 °C, the peaks at 2θ of 13.1° and 27.1° corresponding to the formation of g- C_3N_4 (at 600 °C) are completely disappeared. Instead, a new peak at around 26.0° emerges, which represents the formation of amorphous carbon with the (002) phase [39, 40]. Raman spectra of NG-T show two featured peaks at 1353 cm^{-1} (D band) and 1576 cm^{-1} (G band), which are assigned to disordered sp^3 carbon and graphitic sp^2 carbon, respectively (Fig. 2b) [41,42]. With the pyrolysis temperature elevated from 700 °C to 1000 °C, the ratio of I_D/I_G is dropped initially, followed by increasing. At 1000 °C, the I_D/I_G value of NG-1000 approaching 1.07 (Fig. 1e), which is caused by the high concentrations of N dopants and abundant defect sites. To understand

the surface area and porosity changes of the NG-T samples calcined at different temperatures ($T = 600\text{--}1000$ °C), N_2 adsorption-desorption analysis is conducted. As presented in Fig. 2c, NG-T exhibits type I and IV isotherms with a H_1 -type hysteresis, which verifies its mesoporous porosity and narrow distribution of porosity [43,44]. The surface area of NG-1000 is determined to be 371 $m^2 g^{-1}$ with an average pore diameter of ~ 3.94 nm. It should be noted that the Pc@ C_3N_4 -600, prepared by mixing Pc and C_3N_4 calcined at 600 °C and Pc-800, prepared by heating Pc at 800 °C give low surface areas (31.2 and 21.8 $m^2 g^{-1}$), which confirms the benefit of employing DCD precursor to significantly increase the surface area and porosity of the N-doped carbon (Table S1).

To determine the N content and surface chemical nature of NG-T catalyst, elemental analysis (EA) and XPS techniques are employed. From the full spectra of NG-T, the typical signals of C1s, N1s, and O1s are identified (Fig. S2). The N content of NG-T determined by EA shows that the N content decreases evidently from 33.68 to 11.03 wt% with the increased pyrolysis temperature (Fig. 1d and Table S2). The significant decrease of N content in NG-1000 catalyst can be ascribed to the high-temperature escaping effect [45–47]. Particularly, the pyridinic-N decreases visibly, leaving more stable graphitic-N species (Fig. 3f). The high-resolution N1s spectra are deconvoluted to confirm the bonding configuration and the population changes of N species in NG-T. As shown in Fig. 3, the pyrrolic- and pyridinic-N in Pc parent are relatively stable below 600 °C, however, above 800 °C the pyrrolic-N begins to vanish while the graphitic-N emerges. Thus, the N-species identified in NG-T between 800–1000 °C are mainly pyridinic- and graphitic-N [48]. Under this circumstance, the influence of pyridinic-, pyrrolic- and graphitic-N on CO_2RR can be well differentiated based on different pyrolysis temperatures.

3.2. Evaluation of CO_2RR performance of NG-T catalyst

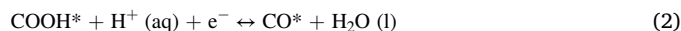
To illustrate the excellent catalytic performance of the large surface area N-doped graphene-like carbon (NG-T) catalyst, the electrochemical CO_2RR catalytic activity of NG-T is analyzed in CO_2 -saturated 0.5 M $KHCO_3$ electrolyte. As shown in Fig. S5a, the cyclic voltammetry (CV) of NG-1000 displays an enhanced cathodic current density and a positive shift in onset potential in CO_2 protected atmosphere as compared to the N_2 -saturated solution. Linear sweep voltammetry (LSV) in Fig. 4a exhibits the electrocatalytic activity of NG-T and Pc/CNTs catalysts. The results show that both NG-900 and NG-1000 have high catalytic activity by generating more than 10 $mA cm^{-2}$ current densities at -0.77 V versus RHE. The liquid and gas products are determined by 1H nuclear magnetic resonance spectroscopy (NMR) and gas chromatography (GC),

respectively. As shown in Fig. S3, no liquid products are detected, indicating that CO is the only product in the CO₂RR process. The CO selectivity is presented in Fig. 4b. Firstly, NG-700 is investigated, and it showed nearly zero selectivity towards CO₂RR but 100 % Faradaic efficiency (FE) towards reducing water into H₂ at the potential range from -0.57 to -0.97 V vs. RHE. Surprisingly, the CO Faradaic efficiency is significantly increased to 88.0 %~94.5 % in the potential range of -0.72~-0.87 V vs. RHE for NG-800 catalyst. The NG-900 and NG-1000 catalysts display a wider range of potentials (-0.57~-0.87 V) and higher partial current density in converting CO₂ into CO in contrast to the NG-800. Moreover, CO Faradaic efficiency reaches a maximum value of 95.0 % at -0.72 V vs. RHE, with the CO current density of 9.07 mA cm⁻², which is superior in comparison with other free-metal catalysts (Table S3). For instance, the current density of the catalyst is about 2.4~88 times that of literature reported results and FE_{CO} reaches the highest level reported so far (Fig. 4d). Significantly, it also possesses a wider potential range (0.57~0.87 V vs. RHE) with the FE_{CO} consistently higher than 85 % compared with other free metals. The high activity of NG-T catalysts can be explained by the following reasons: Firstly, higher N dopant concentrations and large porosity benefited from the DCD precursor strategy. Secondly, more graphite N active species are presented in the calcined samples in NG-900 and NG-1000. Lastly, the ultrathin graphene-like planar structure and N-rich structure facilitate the charge transfers, thus improve the catalytic performance. In addition, electrochemical stability is another important criterion to evaluate the catalyst performance in CO₂RR. Herein, the metal-free NG-1000 catalyst displayed a relatively high current density of -8.41 mA cm⁻² during the 10 h electrolysis. Although the CO Faradaic efficiency was slightly decreased to 79.5 %, it is still close to the best results in literature, illustrating comparable good stability (Table S3). The slight decrease of the F_{CO} may be due to the transition of CC to CO and the adsorbed F-containing species that derived from the Nafion binder during the electrolysis process (Figs. S6 and S7).

3.3. Identification of the active site of NG-T catalyst

In order to identify the actual reactive N species during the CO₂RR process, pure Pc molecule is loaded on CNTs using the wet impregnation method as for Pc/CNTs, which only shows a 2.1 % Faradaic efficiency of CO at the potential of -0.72 V versus RHE. From this result, it is reasonable to conclude that the contribution of pyrrolic- and pyridinic-N in the phthalocyanine ring towards selectively CO₂RR is negligible. Additionally, the Faradaic efficiency towards H₂ evolution of the NG-700 electrode is always greater than 98.6 % within the studied potential range, indicating that the pyrrolic-N is only beneficial for competitive hydrogen evolution reaction. To further confirm the role of pyridinic-N, 1.0 M H₃PO₄ aqueous solution was used to treat the pyridinic-N species in NG-1000 catalyst. The phosphate anions tend to be selectively adsorbed at pyridinic-N sites, and blocking the interaction between CO₂ molecule and pyridinic-N species.²¹ The H₃PO₄ adsorbed NG-1000 demonstrates similar electrocatalytic activity and selectivity towards CO₂RR, suggesting that the pyridinic-N, similar to as pyrrolic-N, is inactive for CO₂RR (Fig. S4). Thus, the active site of NG-1000 catalyst is likely to be graphitic-N doped carbon. Furthermore, such experimental results correlated well with the distribution of N species in the XPS spectra of NG-T catalyst. With the increase of the pyrolysis temperature from 700 to 1000 °C, the relative content of pyridinic-N decreases significantly. However, in the potential window the high CO selectivity is well maintained with the increased pyrolysis temperature. In contrast, the increasing trend of graphitic-N is consistent with the improved CO₂RR performance, indicating the graphitic-N may be the main active species. From a more profound perspective, the above results also inspire us that the contribution of N species, especially graphitic-N or its adjacent C atoms, to the electrocatalytic CO₂RR should not be ignored for carbon-based catalytic materials synchronously doped with N and metal active sites.

To further understand the reaction mechanism and real active sites of electrocatalytic CO₂RR for NG-1000 catalyst, we carried out density functional theory (DFT) calculations based on the computational hydrogen electrode (CHE) model [49]. The mechanism involves two proton-coupled-electron-transfer steps with *COOH and *CO as intermediates, respectively, and the reaction steps are shown below [50].



where * represents the active sites on the substrate. The free energy diagram of CO₂RR to CO on NG-1000 at 0 V and -0.72 V vs. RHE are shown in Fig. 5. The potential-limiting step is the formation of adsorbed COOH* with an overpotential of 0.82 eV (-0.72 V vs. RHE). The most stable structures of *COOH and *CO adsorbed on NG-1000 catalyst were determined by relaxing different possible configurations (Fig. 6). It is found that the actual active sites for CO₂RR on NG-1000 is the C atoms next to the graphitic-N species rather than the pyrrolic-, pyridinic- and graphitic-N, in agreement with the experimental results [26].

4. Conclusions

In summary, a soft template-assisted strategy is successfully developed to fabricate high surface area, highly concentration N-doped carbon catalysts. Furthermore, the N species in the catalyst can be well adjusted by pyrolysis temperatures. The average thickness of the graphene-like carbon is about 7-8 layers of graphene, confirming the feasibility of such a soft template-assisted strategy. It should be noted that our home-made catalyst can not only accurately distinguish between different N species but also possess an increased conductivity and a large number of active sites. Combined with the evolution of N species in NG-T catalysts and electrocatalytic CO₂RR, a convincing conclusion can be drawn that the active sites should be C atoms adjacent to the graphitic-N species. Meanwhile, the results of NG-700 and H₃PO₄-treatment NG-1000 electrocatalytic experiments reveal that the contributions of pyrrolic- and pyridinic-N are negligible. Overall, such metal-free N-doped graphene-like carbon is a preferential alternative to the existing metal-based catalysts for renewable CO₂ fixation and conversion. In the future, we will further explore the functions of heteroatoms dopants for improving the catalytic performance, identifying the possible actual active site and rational design of these catalysts.

CRedit authorship contribution statement

Jingjing Li, Wen-Yan Zan, Hongxing Kang, Zhengping Dong, Xiaoming Zhang, Yixiong Lin, Yue-Wen Mu and Fengwei Zhang: Conduct the experiments, analyse and plot the data; **Fengwei Zhang, Xian-Ming Zhang and Jing Gu:** Conceive the experiments, validation, writing the manuscript, reviewing and editing.

Declaration of Competing Interest

The authors report no declarations of interest.

Acknowledgements

Fengwei Zhang and Xianming Zhang want to acknowledge National Natural Science Foundation of China (21703129, 221173137) for support this research. In addition, they are also very grateful for the test platform provided by scientific instrument center of Shanxi University.

Appendix A. Supplementary data

Supplementary material related to this article can be found, in the

online version, at doi:<https://doi.org/10.1016/j.apcatb.2021.120510>.

References

- [1] D.F. Gao, R.M. Aran-Ais, H.S. Jeon, B. Roldan Cuenya, Rational catalyst and electrolyte design for CO₂ electroreduction towards multicarbon products, *Nat. Catal.* 2 (2019) 198–210.
- [2] K. Chen, J. Deng, J. Zhao, X. Liu, S. Imhanria, W. Wang, Electrocatalytic production of tunable syngas from CO₂ via a metal-free porous nitrogen-doped carbon, *Ind. Eng. Chem. Res.* 60 (2021) 7739–7745.
- [3] Y.Y. Birdja, E. Perez-Gallent, M.C. Figueiredo, A.J. Gottle, F. Calle-Vallejo, M.T. M. Koper, Advances and challenges in understanding the electrocatalytic conversion of carbon dioxide to fuels, *Nat. Energy* 4 (2019) 732–745.
- [4] Y.S. Wu, Z. Jiang, X. Lu, Y.Y. Liang, H.L. Wang, Domino electroreduction of CO₂ to methanol on a molecular catalyst, *Nature* 575 (2019) 639–642.
- [5] J.G. Wu, S.C. Ma, J. Sun, J.I. Gold, C.S. Tiwary, B. Kim, L.Y. Zhu, N. Chopra, I. N. Odeh, R. Vajtia, A.Z. Yu, R. Luo, J. Lou, G.Q. Ding, P.J.A. Kenis, P.M. Ajayan, A metal-free electrocatalyst for carbon dioxide reduction to multi-carbon hydrocarbons and oxygenates, *Nat. Commun.* 7 (2016) 13869.
- [6] Z.D. Li, D. He, X.X. Yan, S. Dai, S. Younan, Z.J. Ke, X.Q. Pan, X.H. Xiao, H.J. Wu, J. Gu, Size-dependent nickel-based electrocatalysts for selective CO₂ reduction, *Angew. Chem. Int. Ed.* 59 (2020) 18572–18577.
- [7] Q. He, D.B. Liu, J.H. Lee, Y.M. Liu, Z.H. Xie, S. Hwang, S. Kattel, L. Song, J.G. Chen, Electrochemical conversion of CO₂ to syngas with controllable CO/H₂ ratios over Co and Ni single-atom catalysts, *Angew. Chem. Int. Ed.* 59 (2020) 3033–3037.
- [8] D.U. Nielsen, X.M. Hu, K. Daasbjerg, T. Skrydstrup, Chemically and electrochemically catalyzed conversion of CO₂ to CO with follow-up utilization to value-added chemicals, *Nat. Catal.* 1 (2018) 244–254.
- [9] J.B. Peng, H.Q. Geng, X.F. Wu, The chemistry of CO: carbonylation, *Chemistry* 5 (2019) 526–552.
- [10] F. Yang, W.H. Hu, C.Q. Yang, M. Patrick, A.L. Cooksy, J. Zhang, J.A. Aguiar, C. C. Fang, Y.H. Zhou, Y.S. Meng, J. Huang, J. Gu, Tuning internal strain in metal-organic frameworks via vapor phase infiltration for CO₂ reduction, *Angew. Chem. Int. Ed.* 59 (2020) 4572–4580.
- [11] N. Huang, K.H. Lee, Y. Yue, X.Y. Xu, S. Irle, Q.H. Jiang, D.L. Jiang, A stable and conductive metallophthalocyanine framework for electrocatalytic carbon dioxide reduction in water, *Angew. Chem. Int. Ed.* 59 (2020) 16587–16593.
- [12] Y. Zhang, W. Zhang, Y. Feng, J. Ma, Promoted CO₂ electroreduction over indium-doped SnP₃: a computational study, *J. Energy Chem.* 48 (2020) 1–6.
- [13] Z.-X. Wei, Y.-T. Zhu, J.-Y. Liu, Z.-C. Zhang, W.-P. Hu, H. Xu, Y.-Z. Feng, J.-M. Ma, Recent advance in single-atom catalysis, *Rare Metals* 40 (2021) 767–789.
- [14] L. Lin, H.B. Li, C.C. Yan, H.F. Li, R. Si, M.R. Li, J.P. Xiao, G.X. Wang, X.H. Bao, Synergistic catalysis over iron-nitrogen sites anchored with cobalt phthalocyanine for efficient CO₂ electroreduction, *Adv. Mater.* 31 (2019), 1903470.
- [15] E.H. Zhang, T. Wang, K. Yu, J. Liu, W.X. Chen, A. Li, H.P. Rong, R. Lin, S.F. Ji, X. S. Zheng, Y. Wang, L.R. Zheng, C. Chen, D.S. Wang, J.T. Zhang, Y.D. Li, Bismuth single atoms resulting from transformation of metal-organic frameworks and their use as electrocatalysts for CO₂ reduction, *J. Am. Chem. Soc.* 141 (2019) 16569–16573.
- [16] Q. He, J.H. Lee, D.B. Liu, Y.M. Liu, Z.X. Lin, Z.H. Xie, S. Hwang, S. Kattel, L. Song, J.G. Chen, Accelerating CO₂ electroreduction to CO over Pd single-atom catalyst, *Adv. Funct. Mater.* 30 (2020), 2000407.
- [17] A.G.A. Mohamed, Y.Y. Huang, J.F. Xie, R.A. Borse, G.J. Parameswaram, Y.B. Wang, Metal-free sites with multidimensional structure modifications for selective electrochemical CO₂ reduction, *Nano Today* 33 (2020), 100891.
- [18] J.F. Xie, X.T. Zhao, M.X. Wu, Q.H. Li, Y.B. Wang, J.N. Yao, Metal-free fluorine-doped carbon electrocatalyst for CO₂ reduction outcompeting hydrogen evolution, *Angew. Chem. Int. Ed.* 57 (2018) 9640–9644.
- [19] H.P. Yang, Y. Wu, Q. Lin, L.D. Fan, X.Y. Chai, Q.L. Zhang, J.H. Liu, C.X. He, Z. Q. Lin, Composition tailoring via N and S co-doping and structure tuning by constructing hierarchical pores: metal-free catalysts for high-performance electrochemical reduction of CO₂, *Angew. Chem. Int. Ed.* 57 (2018) 15476–15480.
- [20] B.B. Pan, X.R. Zhu, Y.L. Wu, T.C. Liu, X.X. Bi, K. Peng, N. Han, J. Zhong, J. Lu, Y. F. Li, Y.G. Li, Toward highly selective electrochemical CO₂ reduction using metal-free heteroatom-doped carbon, *Adv. Sci.* 7 (2020), 2001002.
- [21] J.X. Shan, X.Q. Sun, S.Y. Zheng, T.D. Wang, X.W. Zhang, G.Z. Li, N-dominated nitrogen-doped carbon nanotubes as efficient metal-free catalysts for hydrogenation of nitroarenes, *Carbon* 146 (2019) 60–69.
- [22] Q. Sun, X.Y. Song, L. Gao, W. Chen, Y.M. Li, L.Q. Mao, J.H. Yang, Heterogeneous liquid phase oxidation of ethylbenzene to acetophenone with graphene carbon-based catalyst, *Chem. Pap.* 72 (2018) 2203–2214.
- [23] N.D. Shcherban, P. Mäki-Arvela, A. Aho, S.A. Sergienko, P.S. Yaremov, K. Eranen, D.Y. Murzin, Melamine-derived graphitic carbon nitride as a new effective metal-free catalyst for knoevenagel condensation of benzaldehyde with ethylcyanoacetate, *Catal. Sci. Technol.* 8 (2018) 2928–2937.
- [24] C.G. Hu, Y. Lin, J.W. Connell, H.M. Cheng, Y. Gogotsi, M.M. Titirici, L.M. Dai, Carbon-based metal-free catalysts for energy storage and environmental remediation, *Adv. Mater.* 31 (2019), 1806128.
- [25] B. Kumar, M. Asadi, D. Pisasale, S. Sinha-Ray, B.A. Rosen, R. Haasch, J. Abiade, A. L. Yarin, A. Salehi-Khojin, Renewable and metal-free carbon nanofibre catalysts for carbon dioxide reduction, *Nat. Commun.* 4 (2013) 2819.
- [26] P.P. Sharma, J. Wu, R.M. Yadav, M.J. Liu, C.J. Wright, C.S. Tiwary, B.I. Yakobson, J. Lou, P.M. Ajayan, X.D. Zhou, Nitrogen-doped carbon nanotube arrays for high-efficiency electrochemical reduction of CO₂: on the understanding of defects, defect density, and selectivity, *Angew. Chem. Int. Ed.* 54 (2015) 13701–13705.
- [27] S. Liu, H.B. Yang, X. Huang, L.H. Liu, W.Z. Cai, J.J. Gao, X.N. Li, T. Zhang, Y. Q. Huang, B. Liu, Identifying active sites of nitrogen-doped carbon materials for the CO₂ reduction reaction, *Adv. Funct. Mater.* 28 (2018), 1800499.
- [28] Z. Zhang, L. Yu, Y.C. Tu, R.X. Chen, L.H. Wu, J.F. Zhu, D.H. Deng, Unveiling the active site of metal-free nitrogen-doped carbon for electrocatalytic carbon dioxide reduction, *Cell Rep. Phys. Sci.* 1 (2020), 100145.
- [29] X.C. Duan, J.T. Xu, Z.X. Wei, J.M. Ma, S.J. Guo, S.Y. Wang, H.K. Liu, S.X. Dou, Metal-free carbon materials for CO₂ electrochemical reduction, *Adv. Mater.* 29 (2017), 1701784.
- [30] W.Q. Liu, J.W. Qi, P.Y. Bai, W.D. Zhang, L. Xu, Utilizing spatial confinement effect of N atoms in micropores of coal-based metal-free material for efficiently electrochemical reduction of carbon dioxide, *Appl. Catal. B: Environ.* 272 (2020), 118974.
- [31] F.W. Zhang, C. Zhao, S. Chen, H. Li, H.Q. Yang, X.M. Zhang, In situ mosaic strategy generated Co-based N-doped mesoporous carbon for highly selective hydrogenation of nitroaromatics, *J. Catal.* 348 (2017) 212–222.
- [32] P. Zhou, L. Jiang, F. Wang, K.J. Deng, K.L. Lv, Z.H. Zhang, High performance of a cobalt–nitrogen complex for the reduction and reductive coupling of nitro compounds into amines and their derivatives, *Sci. Adv.* 3 (2017), e1601945.
- [33] W.L. He, C.D. Wu, Incorporation of Fe-phthalocyanines into a porous organic framework for highly efficient photocatalytic oxidation of arylalkanes, *Appl. Catal. B: Environ.* 234 (2018) 290–295.
- [34] G. Huang, C. Yan, J.L. Cai, L.Q. Mo, S.H. Zhao, Y.A. Guo, S.J. Wei, Y.L. Shen, Practically efficient ethylbenzene oxidation catalyzed by manganese tetrakis (4-sulfonatophenyl) porphyrin grafted to powdered chitosan, *J. Porphyr. Phthalocya.* 22 (2018) 481–490.
- [35] M. Wang, K. Torbensen, D. Salvatore, S.X. Ren, D. Joulie, F. Dumoulin, D. Mendoza, B. Lassalle-Kaiser, U. Isci, C.P. Berlinguette, M. Robert, CO₂ electrochemical catalytic reduction with a highly active cobalt phthalocyanine, *Nat. Commun.* 10 (2019) 3602.
- [36] L.S. Zhang, S.S. Jie, Z.G. Liu, Bicontinuous mesoporous Co, N co-doped carbon catalysts with high catalytic performance for ethylbenzene oxidation, *New J. Chem.* 43 (2019) 7275–7281.
- [37] X.H. Li, S. Kurasch, U. Kaiser, M. Antonietti, Synthesis of monolayer-patched graphene from glucose, *Angew. Chem. Int. Ed.* 51 (2012) 9689–9692.
- [38] Z.H. Sheng, L. Shao, J.J. Chen, W.J. Bao, F.B. Wang, X.H. Xia, Catalyst-free synthesis of nitrogen-doped graphene via thermal annealing graphite oxide with melamine and its excellent electrocatalysis, *ACS Nano* 5 (2011) 4350–4358.
- [39] M.B. Vázquez-Santos, E. Geissler, K. László, J.N. Rouzard, A. Martínez-Alonso, J.M. D. Tascon, X.R.D. Comparative, Raman, and TEM study on graphitization of PBO-derived carbon fibers, *J. Phys. Chem. C* 116 (2012) 257–268.
- [40] F. Fina, S.K. Callear, G.M. Carins, J.T.S. Irvine, Structural investigation of graphitic carbon nitride via XRD and neutron diffraction, *Chem. Mater.* 27 (2015) 2612–2618.
- [41] Y.F. Lu, S.T. Lo, J.C. Lin, W.J. Zhang, J.Y. Lu, F.H. Liu, C.M. Tseng, Y.H. Lee, C. T. Liang, L.J. Li, Nitrogen-doped graphene sheets grown by chemical vapor deposition: synthesis and influence of nitrogen impurities on carrier transport, *ACS Nano* 7 (2013) 6522–6532.
- [42] S.L. Zhao, M. Li, M. Han, D.D. Xu, J. Yang, Y. Lin, N.E. Shi, Y.N. Lu, R. Yang, B. T. Liu, Z.H. Dai, J.C. Bao, Defect-rich Ni₃FeN nanocrystals anchored on N-doped graphene for enhanced electrocatalytic oxygen evolution, *Adv. Funct. Mater.* 28 (2018), 1706018.
- [43] H. Awala, J.P. Gilson, R. Retoux, P. Boullay, J.M. Goupil, V. Valtchev, S. Mintova, Template-free nanosized faujasite-type zeolites, *Nat. Mater.* 14 (2015) 447.
- [44] J. Gong, B. Michalkiewicz, X.C. Chen, E. Mijowska, J. Liu, Z.W. Jiang, X. Wen, T. Tang, Sustainable conversion of mixed plastics into porous carbon nanosheets with high performances in uptake of carbon dioxide and storage of hydrogen, *ACS Sustain. Chem. Eng.* 2 (2014) 2837–2844.
- [45] P. Sun, J. Huang, F. Xu, J.J. Xu, T.Q. Lin, W. Zhao, W.J. Dong, F.G. Huang, Boron-induced nitrogen fixation in 3D carbon materials for supercapacitors, *ACS Appl. Mater. Interfaces* 12 (2020) 28075–28082.
- [46] Y. Wang, L.H. Chen, Z.X. Mao, L.S. Peng, R. Xiang, X.Y. Tang, J.H. Deng, Z.D. Wei, Q. Liao, Controlled synthesis of single cobalt atom catalysts via a facile one-pot pyrolysis for efficient oxygen reduction and hydrogen evolution reactions, *Sci. Bull.* 64 (2019) 1095–1102.
- [47] P. Bairi, K. Sardar, K. Chanda, M. Samanta, S. Thakur, K. Panigrahi, S. Sarkar, T. Paul, K.K. Chattopadhyay, Shape-shifting via salt crystallization: conversion of a nanostructured polymer into a site-selective nitrogen-doped carbon sheet with enhanced supercapacitive performance, *ACS Appl. Energy Mater.* 3 (2020) 5984–5992.
- [48] Y. Ito, C. Christodoulou, M.V. Nardi, N. Koch, M. Klauhi, H. Sachdev, K. Mullen, Tuning the magnetic properties of carbon by nitrogen doping of its graphene domains, *J. Am. Chem. Soc.* 137 (2015) 7678–7685.
- [49] A.A. Peterson, F. Abild-Pedersen, F. Studt, J. Rossmeisl, J.K. Nørskov, How copper catalyzes the electroreduction of carbon dioxide into hydrocarbon fuels, *Energy Environ. Sci.* 3 (2010) 1311–1315.
- [50] H.A. Hansen, J.B. Varley, A.A. Peterson, J.K. Nørskov, Understanding trends in the electrocatalytic activity of metals and enzymes for CO₂ reduction to CO, *J. Phys. Chem. Lett.* 4 (2013) 388–392.